ACS OMEGA

Open Access

http://pubs.acs.org/journal/acsodf

Article

The Construction of Three-Layered Biomimetic Arterial Graft Balances Biomechanics and Biocompatibility for Dynamic Biological Reconstruction

Han Bao,[‖] Yanyuan Zhang,[‖] He Xin,[‖] Ye Gao, Yan Hou, Guichu Yue, Nü Wang, Yaqiong Wang, Chun Li, Fuwei Liu,* Yong Zhao,* and Liang Kong*

Cite This: *ACS Omega* 2024, 9, 7609−7620

Read Online

ACCESS | Metrics & More | Article Recommendations | Supporting Information

ABSTRACT: The process of reconstructing an arterial graft is a complex and dynamic process that is subject to the influence of various mechanical factors, including tissue regeneration and blood pressure. The attainment of favorable remodeling outcomes is contingent upon the biocompatibility and biomechanical properties of the arterial graft. A promising strategy involves the emulation of the three-layer structure of the native artery, wherein the inner layer is composed of polycaprolactone (PCL) fibers aligned with blood flow, exhibiting excellent biocompatibility that fosters endothelial cell growth and effectively prevents platelet adhesion. The middle layer, consisting of PCL and polyurethane (PU), offers mechanical support and stability by forming a contractile smooth muscle ring and antiexpansion PU network. The outer layer, composed of PCL fibers with an irregular arrangement, promotes the growth of nerves and pericytes for long-term vascular function. Prioritizing the reconstruction of the inner and outer layers establishes a stable environment for intermediate smooth muscle growth. Our three-layer arterial graft is designed to provide the blood vessel with mechanical support and stability through nondegradable PU, while the incorporation of degradable PCL generates potential spaces for tissue ingrowth, thereby transforming our graft into a living implant.

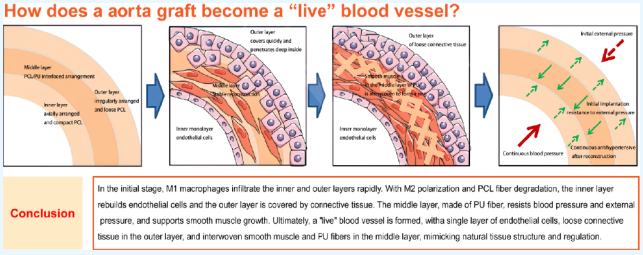

1. INTRODUCTION

There is an increasing demand for arterial grafts for the treatment of traumatic injury, cardiovascular disease, transplantation, and reconstructive surgery.[1] Although autologous grafts have excellent biocompatibility, their source is limited and may lead to issues of additional trauma of normal body.[2] In addition, although saphenous veins are commonly used as arterial grafts, they exhibit different functional and physiological characteristics compared to arteries and lack the resilience to endure arterial pressure, resulting in vascular rupture and posing a life-threatening risk.[3] Artificial aortic grafts have the potential to address the limitation of graft availability and represent the future direction for clinical applications.[4] Presently, polytetrafluoroethylene (PTFE) arterial grafts are widely employed in clinical treatments. Nevertheless, these grafts lack metabolic or remodeling capabilities within the body. Functioning solely as conduits for blood flow, they exhibit limited interaction or integration with surrounding tissues, having the possibility of aging-related changes in the long run, which could influence the prognosis.[5] Current research has made partial improvements in the structure or functionality of artificial blood vessels by using biodegradable synthetic materials such as polycaprolactone (PCL) and polylactic acid (PLA), but compared to natural vessels, there are shortcomings in directing cell growth or simulating the supporting strength of natural vessels.[6,7] An alternative strategy involves employing decellularized natural blood vessel grafts, typically sourced from animal or human tissues. These grafts demonstrate commendable biocompatibility and possess the ability to induce tissue regeneration. Nonetheless, being of organic origin, there exists a potential risk such as disease transmission and immune reactions.[8] Another approach involves the modification of vascular grafts,[9] such as constructing nanotopography on the inner surface of the vessels, incorporating VEGF, or introducing stem cells derived from perivascular adipose tissue to further enhance the remodeling effects of artificial vascular grafts in vivo.[10,11]

The in vivo reconstruction of the arterial graft is a dynamic process that involves not only promoting tissue growth but also, more crucially, strategically orchestrating the sequential growth of different tissues. It requires restraining the rapid growth of specific tissues while providing the essential

Received: September 3, 2023
Revised: December 24, 2023
Accepted: January 15, 2024
Published: February 9, 2024

environment and support for the slower-growing ones.[12] Due to the exposure to the dynamic environment created by blood pressure, arterial grafts not only need to exhibit excellent biocompatibility but also require mechanical strength that mimics the natural vasculature to support blood pressure stability.[13] The structure of natural arterial vessels consists of the inner, middle, and outer layers. The outer layer's pericytes maintain and repair vascular integrity. Nerves control smooth muscle contraction in the middle layer, regulating vascular tone.[14] Collaborating with the antidilatation elastic membrane, the outer layer stabilizes blood pressure, sustaining inner layer endothelial cell to preserve permeability, prevent thrombosis, and promote long-term blood vessel patency.[15] Therefore, improving the biocompatibility alone may not fully meet the criteria for in vivo remodeling.

Therefore, this study aimed to mimic the inner, middle, and outer three-layer structures of the native artery to fulfill the dynamic requirements of biocompatibility and biomechanical properties in the reconstruction process. In this study, a biomimetic three-layer nanofiber vascular graft was developed by electrospinning. The inner layer of PCL fiber followed the direction of blood flow, had adequate biocompatibility, promoted endothelial cell growth,[16] and effectively prevented platelet adhesion, erythrocyte aggregation, and thrombosis. The middle layer of the PCL/polyurethane (PU)-interlaced arrangement provided mechanical support and finally formed a contractile smooth muscle ring and antiexpansion PU network to maintain long-term resistance stability. Additionally, the outer layer of irregularly arranged PCL fibers was conducive to the growth of nerves and blood vessels to protect the long-term function of blood vessels. At the same time, the priority reconstruction of the inner and outer layers also contributed to a stable biological microenvironment for the growth of the middle layer smooth muscle, and the interlaced arrangement increased its porosity during middle layer reconstruction, providing a scaffold template for the growth of smooth muscle cells. Dynamic reconfiguration of the vascular graft in vivo allowed the formation of a "living" vessel with the three-layer structure and function of the native artery.

2. METHODS

2.1. Material Preparation and Morphological Characterization. *2.1.1. Production of Electrospinning Artificial Blood Vessel.* We used a preprepared PCL mixed solution, which was thoroughly mixed for an additional 30 min before use to ensure complete dissolution of PCL. The solution was collected using a 2 mL syringe and fed into the electrospinning system. The collection system featured a 10 cm metal roller with a 2 mm diameter, and the spinning nozzle was positioned approximately 15 cm above the collection roller. An electric voltage of 10 kV was maintained with the roller parallel to the ground and the spinning nozzle perpendicular to the ground. The motor speed was adjusted to 1200 rpm, and spinning was conducted at a temperature of 25 °C and a relative humidity of 50%. After 2 h, the material was collected to obtain the innermost layer of the artificial blood vessel.

The PCL/PU mixed solution was collected in a 2 mL syringe, replacing the syringe previously used for the PCL mixed solution. It was placed within the electrospinning system, and a microinfusion pump was set to advance at a rate of 1 mL/h. The motor speed was adjusted to 2000 rpm, and after 5 h, the material was collected, resulting in the formation of a double-layered artificial blood vessel.

Continuing with the PCL mixed solution, it was placed in the electrospinning system with the motor speed set at 2000 rpm. After 3 h, the material was collected. Subsequently, it was placed in a vacuum drying oven for 24 h to allow complete solvent evaporation. The material was stored at room temperature for future use.

2.1.2. Cross-Sectional SEM Observation. The artificial blood vessel was subjected to a cryogenic treatment by immersion in liquid nitrogen for 1 min. Subsequently, a pair of forceps was employed to securely hold the artificial blood vessel, which was then pressed to the bottom of a beaker and precisely sectioned using a scalpel. Each resulting cross-sectional segment measured approximately 0.5 cm in length. To ensure structural integrity, sections were handled with care and were not touched by hand. Following this, the artificial blood vessel underwent a gold coating before being subjected to microscopic analysis via a scanning electron microscope. Multiple observations were made, images were captured, and data were recorded. This entire process was performed in five replicates for each sample.

For the natural blood vessels, Sprague–Dawley (SD) rats were anesthetized and euthanized using an overdose of intraperitoneal sodium pentobarbital injection. The abdominal aorta was then isolated, thoroughly washed with phosphate-buffered saline (PBS) three times, and fixed in a 4% glutaraldehyde fixative solution. The specimens were refrigerated at 4 °C overnight. To prepare cross-sectional samples, the natural blood vessels were subjected to cryogenic treatment by immersing them in liquid nitrogen for 1 min. Subsequently, two tweezers were utilized to break the natural blood vessel to a length of 0.5 cm, while ensuring that the cross-sectional integrity was maintained. The samples were then sequentially immersed in 30%, 50%, 70%, 80%, and 90% ethanol solutions for dehydration, followed by two rounds of dehydration in absolute ethanol for 15 min each. Subsequently, the samples were immersed in osmium tetroxide, left to soak for 2 h, and then gold-coated. Cross-sectional observations were conducted via scanning electron microscopy, and multiple images were taken and recorded. Each step in this process was repeated five times for each sample.

2.2. Blood Compatibility Test. *2.2.1. Erythrocyte Aggregation.* The artificial blood vessels were cut into 1 cm in length for prepared. The blood of the middle auricular artery of New Zealand white rabbits was taken for 30 mL and stored in six heparin anticoagulant tubes (5 mL/every tube, $n = 5$). Taken an above tube and put into an artificial vessel is the experiment group, and the tube with 1 mL of normal saline added is the control group, which was repeated 3 times in each group. The samples were flipped gently, so that the blood was in complete contact with the artificial vessel. After 30 min, a small amount of blood was absorbed and made into a blood smear. The aggregation of red blood cells was observed under a microscope and photographed, to evaluate the effect of vascular samples on erythrocyte aggregation.

2.2.2. Platelet Adhesion Detection. The sterilized artificial vascular diaphragm was cut into a 1×1 cm^2 square patch ($n = 5$) and placed at the bottom of the cell culture dish and soaked in PBS to make its surface moist. Fresh blood from the middle auricular artery of New Zealand rabbits was collected for 10 mL (heparin, anticoagulant), centrifuged for 10 min (2700 rpm), and then the platelet-rich plasma (PRP) was collected in a clean silicified test tube. The artificial vascular slices from PBS were taken out, put into fresh PRP, and incubated at 37

https://doi.org/10.1021/acsomega.3c06628
ACS Omega 2024, 9, 7609−7620

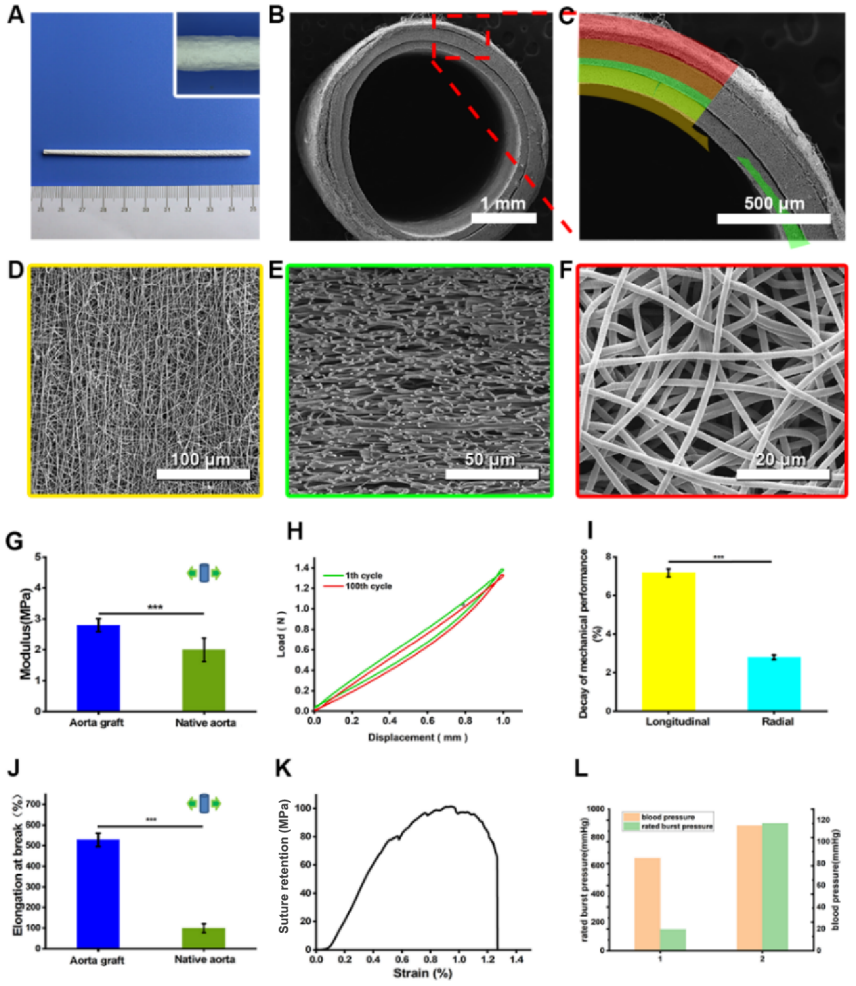

Figure 1. Construction and mechanical characterization of the biomimetic blood vessel. A. Optical image of the artificial blood vessel. B, C. Scanning electron microscopy (SEM) image of the three-layer structure of the cross-sectional artificial blood vessel. D. SEM image depicts the inner layer. E. SEM image displaying the fiber structure of the middle layer. F. SEM image of the outer layer. G. Radial tensile stress−strain curve and elastic modulus of the aorta graft. H, I. Fatigue cycle curve showing the radial attenuation of the artificial blood vessel. J. Radial elongation at break. K. Stress−strain curve of the zigzag suture strength. L. Relationship between blasting strength and blood pressure.

°C for 4 h. Taken out the sample, washed 1 min with PBS, fixed with 4% glutaraldehyde overnight, then soaked in 30%, 50%, 70%, 80%, and 90% ethanol, respectively, and dehydrated twice in anhydrous ethanol for 15 min each time. Then, put it in an osmic acid dish, immerse it, and place in the ventilation cabinet for 2 h. After osmic acid volatilizing completely, spraying was performed, and then the artificial vascular diaphragm was observed under SEM, to evaluate the effect of vascular samples on platelet adhesion.

2.3. Mechanical Characterization. *2.3.1. Antifatigue Test.* The artificial blood vessel was observed via scanning electron microscopy to obtain cross-sectional images, and the thickness of the vessel was measured from eight different positions using ImageJ software. The average thickness (d) was then calculated. The vessel was cut into a sheet, and the width (w) was measured by using a vernier caliper. The universal instrument was used to fix the head and measure the distance. The vessel was subjected to a cyclic deformation of 20% with 100 cycles at a pulling speed of 1 cm/min. Measure axial and radial cycle data separately with five measurements each. Record stretched length ΔL and tensile force value F were recorded for each measurement. Use the formula to obtain preliminary results and analyze them using Origin 9.

$$\sigma = F/S = F/(d \cdot w)$$

$$\varepsilon = \Delta L/L_0 = (L_X - L_0)/L_{0_{*100\%}}$$

$$\text{Elongation at Break}^{\%} = (L_B - L_0)/L_{0*100\%}$$

Here, σ: Stress; F: Tensile Force; S: Area; d: Length; w: Width; ε: Strain; L_x: Elongation; L_0: Length of Artificial Blood Vessel; L_B: Elongation at Break.

2.3.2. Burst Pressure Test. We developed a specialized instrument for measuring the burst pressure in artificial blood vessels. The instrument used a three-way interface connecting an electronic barometer, a gas cylinder, and an artificial blood vessel for uniform pressure distribution. The vessel was positioned lower to prevent water backflow and instrument damage. A dropper bottle was connected to one end of the vessel and the three-way device to the other. To measure burst pressure, the vessel was filled with double distilled water, and the gas cylinder was gradually introduced to increase the barometer reading until rupture occurs. The barometer reading at rupture was recorded.

https://doi.org/10.1021/acsomega.3c06628
ACS Omega 2024, 9, 7609−7620

2.3.3. Suture Strength Test. Cut the artificial blood vessel to a 1 cm length, mark a point 1 mm from the edge using a vernier caliper, and pass an 8−0 microsurgical suture through the mark to form a loop. Fix one end of the vessel to the lower end of a universal instrument using the instrument's chuck, and fix the other end to the upper chuck using the suture. Measure the stretched length and tensile force value while recording the data.

2.3.4. Porosity Test. We immersed the samples separately in type I and type III collagenases for 6 h each to ensure complete dissolution of the extracellular matrix. Following this enzymatic treatment, we carried out a two-step dehydration process in a gradient of ethanol, each step lasting 15 min, followed by dehydration in absolute ethanol. The samples were then placed in dishes containing osmium tetroxide and left in a fume hood for 2 h to allow for the complete volatilization of osmium tetroxide. Subsequent to this, a gold coating was applied, and scanning electron microscopy was employed to visualize the surface microstructure of the material. Utilizing ImageJ software, we analyzed the images, determined the scale, defined the spinning range, calculated pore size and quantity, and generated corresponding result figures to illustrate the material's degradation.

2.4. Surgery Process In Vivo, Time Point of Material Sampling, and General Observation. Thirty 8-week-old male SD rats (200−230 g) were obtained from the Animal Experiment Center of the Air Force Military Medical University. All animal experiments comply with the National Institutes of Health guide for the care and use of Laboratory animals. Rats were anesthetized with an intraperitoneal pentobarbital injection. After anesthesia and disinfection, a midline incision exposed the abdominal aorta and vena cava. The aorta was separated, clamped, and flushed with sodium heparin. The artificial blood vessel (6−8 mm) was sutured to the aorta using 8−0 microsurgery, with 10−12 stitches per anastomosis. Blood flow was restored by releasing the distal clip. Additional sutures were added for excessive bleeding. The proximal clip was released, observing the implanted vessel's pulsation. The abdominal cavity was flushed with saline and closed. No anticoagulants or antibiotics were administered. Samples were collected at 1, 3, and 6 months postsurgery. Rats were euthanized at 30, 90, and 180 days using intraperitoneal sodium pentobarbital injection. Implants and surrounding tissues were removed, washed with PBS, and photographed with a stereomicroscope.

2.5. Color Doppler Ultrasound and Abdominal Aortic Angiography. Rats underwent Doppler ultrasound at 30, 90, and 180 days postoperation. Prior to the examination, rats were fasted for 6 h, deprived of water for 2 h, and anesthetized with intraperitoneal pentobarbital sodium. Sodium pentobarbital was injected into the abdominal cavity of rats. Gray-scale imaging in transverse and longitudinal sections assessed the abdominal aorta structure. Color Doppler flow imaging technology examined blood flow filling, velocity, and flow conditions. At 180 days postsurgery, Micro-CT abdominal aortogram assessed the patency of artificial blood vessels. Rats were anesthetized with pentobarbital sodium, and organ flushing used heparin sodium saline. MICROFIL contrast agent enabled blood vessel visualization, with Micro-CT scans performed from the xiphoid process to the symphysis pubis level. Reconstructed cross-sectional images provided angiographic visualization, with high-density shadow areas, indicating successful perfusion.

3. RESULTS

3.1. Construction of a Three-Layer Bionic Structure. An artificial arterial graft mimicking the three-layer structure of the native aorta was designed through layer electrospinning, which is anticipated to enhance the reconstructive effect from a bionics perspective (Figure 1A−C). The inner layer of the artificial blood vessel was made of PCL, an FDA-approved biomaterial known for its biocompatibility and ease of modification, to enhance its biological activity, making it a suitable material for clinical applications. The scanning electron microscopy (SEM) examination reveals a compact arrangement of the inner fiber structure, aligned parallel to the longitudinal axis of the blood vessel, exhibiting a uniform pore distribution (Figure 1D). Aligning the fibers in the direction of blood flow improved the biocompatibility of the artificial blood vessel, minimized the risk of embolism, and promoted the orderly and directional growth of endothelial cells.

The fiber structure of the middle layer was observed using SEM. It consisted of PCL and PU, which provided mechanical strength for the vessel wall. PCL is a biocompatible material with proven clinical applications, characterized by its degradability and safety.[17,18] As PCL was progressively degraded, it acted as a scaffold for uniform and organized growth of smooth muscle cells, aiding in maintaining the circular shape of the vessel wall and preventing alterations in the shape during contraction. Meanwhile, the PU component formed an annular mesh structure mimicking the native aorta's elastic membrane, regulating blood pressure by preventing excessive expansion (Figure 1E). The PU network structure provided a simple and effective strategy for integrating the elastic membrane with the surrounding tissue, despite the challenges of replicating the complex extracellular matrix (ECM) of the elastic membrane.

The outer layer exhibits a disorganized morphology, as observed through scanning electron microscopy (Figure 1F), accelerating the adhesion and proliferation of fibroblasts, vascular pericytes, and nerve cells, which is essential for the development of "living" blood vessels mediated by the body's physiological functions. The artificial blood vessel consisted of an inner layer with a thin endothelial layer, a middle layer with a smooth muscle layer, and an outer layer with a loose connective tissue layer. The thickness of the inner layer was $1.45 \pm 0.60\ \mu$ m, that of the middle layer was $66.69 \pm 4.0\ \mu$m, and finally, that of the outer layer was $115.28 \pm 24.51\ \mu$m. The inner and outer layers prioritized contact with the surrounding tissue for biological remodeling,[19] providing a stable growth environment for the slow-growing smooth muscle cells in the middle layer (Figure 1G). SEM images illustrated that the dense and uniform inner fibers, interlaced middle layer, and outer layer collectively promoted cell growth. We obtained stress−strain curves in both the longitudinal and radial directions of the artificial blood vessel, subjected to 20% elongation for 100 cycles (Figures 1H, S1B). A comparison of the two curves reveals that the radial stress−strain curve exhibited a relatively smaller change, with a decay of approximately 7%, while the longitudinal curve experienced a more substantial variation, with a decay of about 13% (Figure 1I), and its elongation at break could extend to $564 \pm 28.00\%$ (Figure 1J). At the same time, the zigzag suture strength displayed a maximum strength of 101.42 ± 18.55 MPa (Figure 1K), and the artificial blood vessel could withstand a pressure

https://doi.org/10.1021/acsomega.3c06628
ACS Omega 2024, 9, 7609−7620

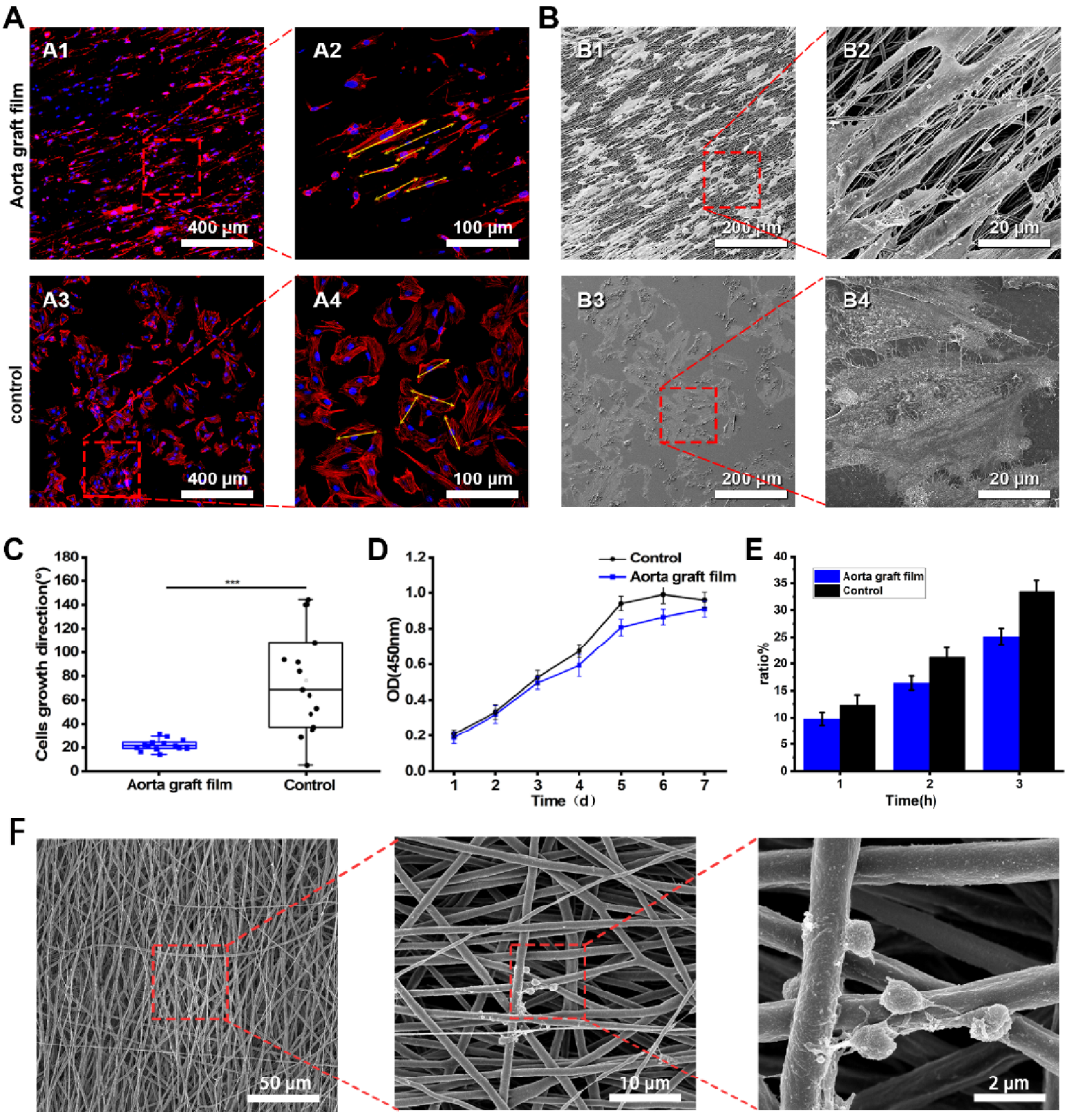

Figure 2. Effect of the inner layer on endothelial cells in vitro. A: A1,A2. Confocal microscopy image showing spindle-shaped endothelial cells in the artificial blood vessel with a spinning arrangement of the cytoskeleton. A3,A4. In contrast, the control group exhibits an irregular arrangement. B: B1,B2. SEM images showing elongated endothelial cells with lamellar pseudopods in the artificial blood vessel aligned along the spinning arrangement. B3,B4. In contrast, endothelial cells in the control group exhibited a paving stone-like appearance with radial filopodia. C. Cell distribution angle statistics and D. CCK8 assay detecting the cell proliferative ability of SVARECs. E. Blood smear observation and statistics of the red blood cell aggregation ratio. F. Electron microscopy scanning of platelet adhesion.

of at least 900 mmHg without leakage (Figure 1L), indicating potential clinical applications.

3.2. Biocompatibility Test of the Inner Layer. In addition to successfully constructing the three-layer biomimetic structure, we conducted an in vivo and in vitro study to evaluate its remodeling. In our research, we used the electrospinning technology of the three layers to mimic the ECM, aligning it with the distribution of collagen fibers in blood vessels. This microstructure enhanced biocompatibility and provided structural support for the graft, making full use of the advantages of PCL. Vascular endothelial cells are the primary cell type constituting the inner layer of the native aorta.[20] After 7 days of culture, the inner layer of the aorta graft with a nanosequential structure promoted the adhesion and proliferation of vascular endothelial cells SV40-transformed aortic rat endothelial cells (SVARECs), comparable to that of the control group (Petri dish surface), as demonstrated by Cell Counting Kit-8 (CCK-8) assay results (Figure 2D). More importantly, immunofluorescence results revealed that SVAR-ECs on the inner surface of the artificial blood vessel were polarized in the direction of blood flow (Figure 2A). The cell distribution angle analysis showed a significant improvement in cell orientation on the aligned inner layer of the vascular graft (118.3°) compared to that of the control group (139.4°) (Figure 2C). Besides, SEM imaging displayed that cells in the experimental group were densely arranged with increased pseudopodia and intercellular connections (Figure 2B), forming an orderly aggregation of cells that provided favorable conditions for the formation of physiological structural endothelium. Furthermore, fresh blood incubation for 30 min with the artificial vascular slices showed no erythrocyte aggregation caused by the inner layer material (Figure 2E). Platelet adhesion and aggregation are critical in thrombosis. The surface platelet adhesion was observed via scanning

https://doi.org/10.1021/acsomega.3c06628
ACS Omega 2024, 9, 7609−7620

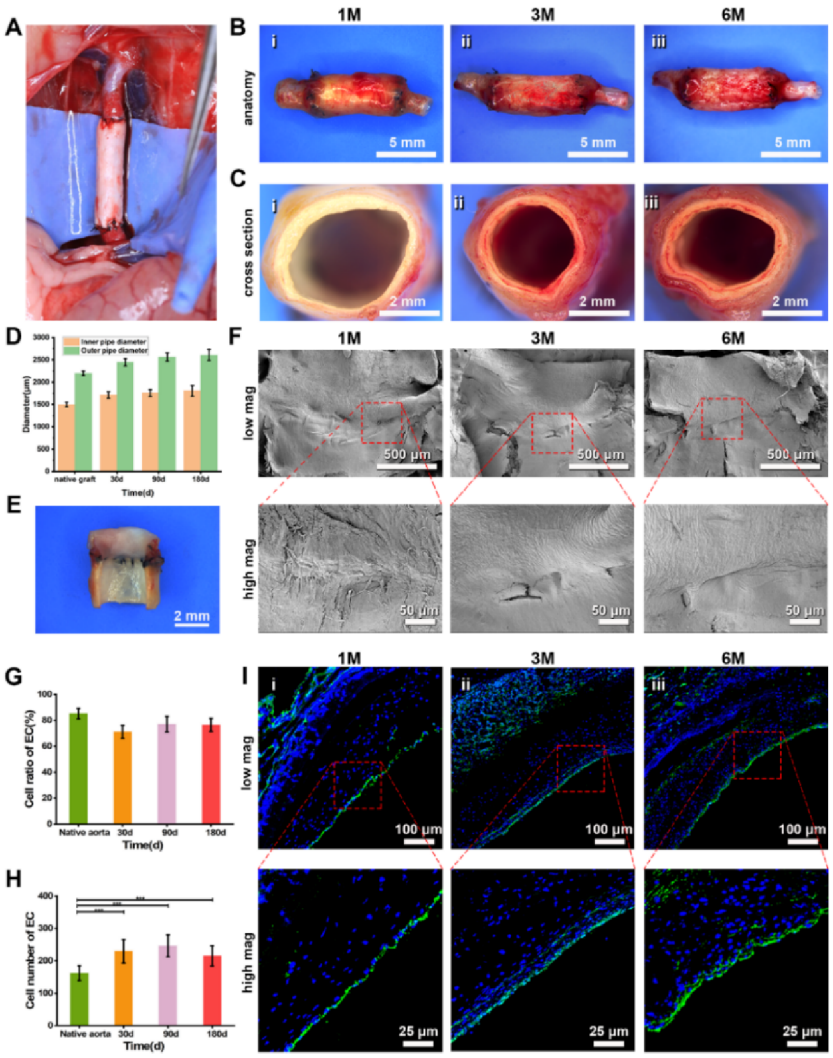

Figure 3. Reconstruction of the inner layer. A. Implanting artificial blood vessels into abdominal aorta defect in rats. B–D. Appearance and cross-sectional appearance and changes in the diameter of the implanted artificial blood vessel in rats at 1, 3, and 6 months following surgery. E,F. Observation and SEM imagery of implanted artificial and natural blood vessel endothelium at suture interface at 1, 3, and 6 months postsurgery. G,H. Percentage of endothelial cell coverage and endothelial cell count of the implanted artificial blood vessel before and 1, 3, and 6 months after surgical intervention. I. Immunofluorescence staining of the implanted artificial blood vessel endothelial cells with CD31 (endothelial cell marker, green) and DAPI (blue) at 1, 3, and 6 months after surgery.

electron microscopy. After multiple searches, platelet adhesion was found in only one of the samples (Figure 2F). The adhered platelets were located at the intersections of multiple fibers and were not in an activated state, appearing spherical with only a minimal extension of pseudopodia. This indicates that this type of artificial blood vessel possesses a certain degree of antiplatelet adhesion effect. These reflected the promising anticoagulation prospect of the inner layer material.

The in vivo remodeling of the bionic vascular graft was observed to integrate well with the surrounding tissues (Figure 3A). Specifically, the graft was implanted into the rat abdominal aorta and retrieved after 30, 90, and 180 days postoperation for further analysis (Figure 3B,C). Adjacent natural endothelium was integrated with the graft without an excessive tissue response (Figure 3E). SEM visualization showed that the 30-day group achieved complete endothelialization of the inner surface of the artificial blood vessel, with lower levels of ECM secretion than the other two groups. Endothelial cells in the 30-day group maintained a native aorta-like orientation despite shrinkage due to dehydration. In the 90-day and 180-day groups, the ECM was significantly increased compared to the 30-day group, and endothelial cells, ECM, and artificial vascular materials were densely packed (Figure 3F). The PCL fibers were degraded, and the reconstruction of the inner and outer layers resulted in a marginally increased inner diameter (1530 ± 134.41 μm to 1821 ± 128.58 μm), validating that the formation of a single-layer vascular endothelium did not affect lumen patency. On the other hand, the outer diameter was significantly increased (2231 ± 207.83 μm to 2763 ± 193.31 μm), signifying that the loose outer fibers facilitated the remodeling of the middle and outer layers (Figure 3D). Immunohistochemistry analysis uncovered a physiological structure of the remodeled endothelium similar to the native vascular endothelial monolayer. A truncated endothelial structure was observed at 30 days, whereas a complete physiological endothelium was visualized at 180 days (Figure 3I). Endothelial cell coverage (Figure 3G) and counts (Figure 3H) indicate that endothelial cells form complete coverage in the inner layer, effectively

https://doi.org/10.1021/acsomega.3c06628
ACS Omega 2024, 9, 7609−7620

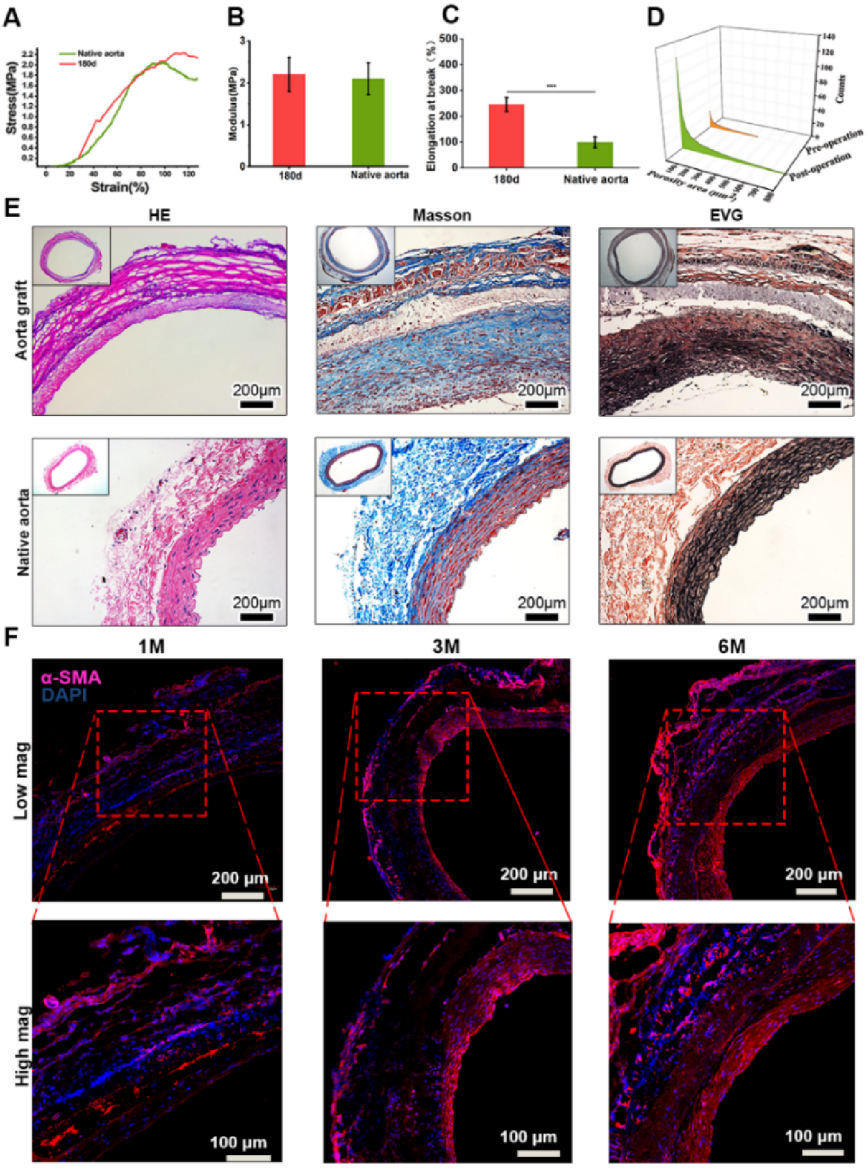

Figure 4. Reconstruction of the middle layer. A. The radial stress−strain curves at the break of the aorta graft and native aorta were compared before and 6 months after surgery. B,C. The radial stress−strain modulus and elongation of the aorta graft and native aorta were investigated 6 months after surgery. D. SEM and surface morphology analysis of the middle layer of artificial blood vessels were conducted pre- and postsurgery. E. The effect of middle layer reconstruction. F. Immunofluorescence staining of α-SMA (smooth muscle cell marker, red) and DAPI (blue) was used to detect smooth muscle cells in artificial blood vessels at 1, 3, and 6 months postsurgery.

reducing platelet adhesion and playing a crucial role in maintaining efficient blood flow.

3.3. Biomechanical Properties Detection of the Middle Layer. Stable mechanical conditions are vital for the regeneration and reconstruction of the body,[21] such as strong internal fixation for fracture healing or tension-reducing sutures for minimizing scarring in soft tissue sutures.[22] Blood vessels are exposed to mechanical forces, including blood pressure, which impacts both microscopic components like endothelial cells and macroscopic conditions such as aneurysms and thrombosis.[23] Previous vascular graft research has not comprehensively addressed the role of the mechanical environment. In our study, electrospinning technology was used to construct a middle layer structure comprising PCL and PU blends, which supported the vascular graft and met the dynamic biomechanical demands during the reconstruction process.

Initial vascular graft stability plays a decisive role in successful implantation.[24] Our study showed that the graft's biomechanical properties were comparable to those of the native aorta, ensuring adequate radial mechanical strength for vascular tissue growth and clinical procedures (Figure 4A). Moreover, the PU/PCL material used in the vascular graft maintained its mechanical strength during degradation, unlike that of other biomaterials. Over time, the graft tissue became more similar to natural blood vessels (Figure 4B,C). At the same time, the porosity of the PCL material increased during degradation (Figure 4D), promoting smooth muscle cell growth, while the annular structure provided a basis for the directional growth and remodeling of smooth muscle. The immunofluorescence results after 1, 3, and 6 months of in vivo implantation (Figure 4F) portrayed that α-SMA-labeled smooth muscle cells initially appeared at 30 days but did not form a complete annular arrangement. However, the number

https://doi.org/10.1021/acsomega.3c06628
ACS Omega 2024, 9, 7609−7620

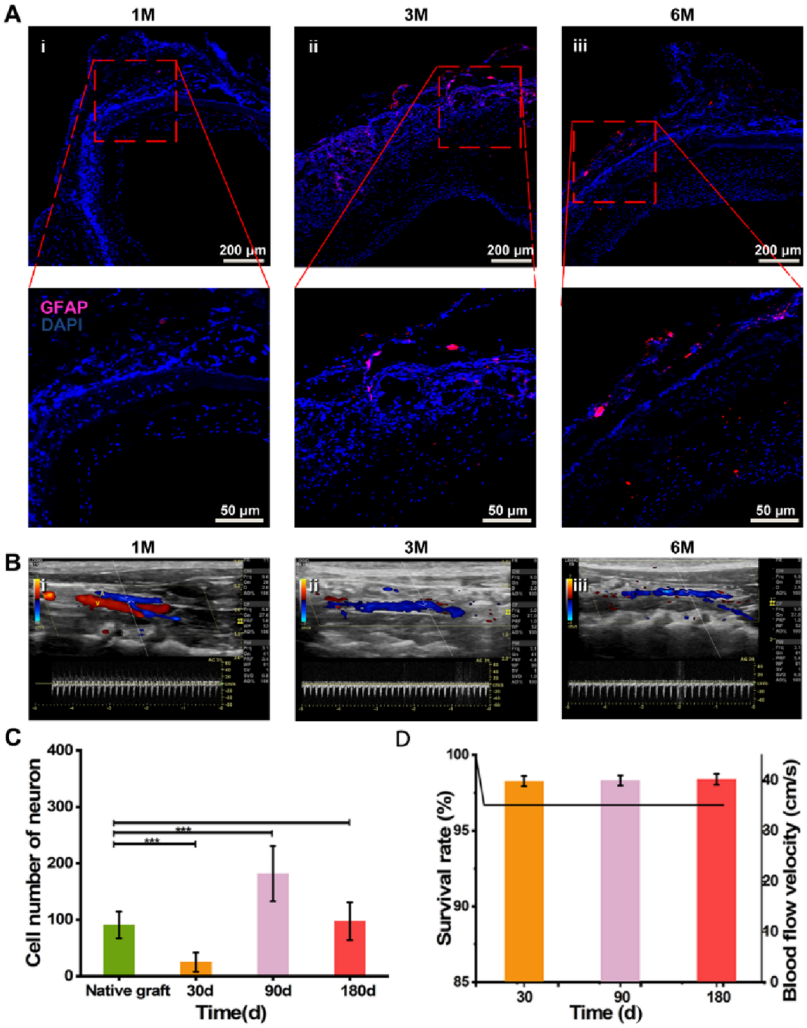

Figure 5. Alteration in the outer layer. A. Artificial blood vessel glial cell immunofluorescence, GFAP (glial cell marker, red), and DAPI (blue) at 1, 3, and 6 months after surgery. B. Color Doppler ultrasound of artificial blood vessels at 1, 3, and 6 months after operation; the blood circulation is unobstructed. C. Image J was employed to count the number of nerve cells. D. Blood flow velocity statistics.

of cells increased over time, and a uniform and directionally arranged annular structure was formed after 180 days, thereby facilitating synchronous and coordinated contraction of blood vessels.

Maintaining vascular compliance is paramount for normal vascular function.[25,26] The elastic membrane in natural blood vessels plays an instrumental role in preventing excessive expansion under high blood pressure conditions.[27] However, the tissue regeneration capacity of pure fibrous tissue is limited, and a complete ring structure is necessitated for proper functioning.[28] Our study found that the PU mesh, together with the smooth muscle ring, acted as an elastic membrane to maintain vascular mechanical stability following PCL degradation. At 180 days postimplantation, only PU existed in the middle layer, and smooth muscle tissue had formed on both the inner and outer sides. Muscle cells were observed infiltrating the material's pores, and it was also noted that the formation of nourishing blood vessels often occurred around the newly generated vessels (Figure 4E), indicating the effectiveness of this design strategy in achieving long-term stability.

3.4. Detection of Outer Nerve Function and Long-Term Patency Rate. Blood vessels are not only channels for blood flow but also "living" tissues that can be regulated by the body.[29] Innervation of the outer layer of blood vessels is central to their proper function and long-term regulation through regeneration and remodeling.[30,31] In our study, the PCL component of the outer layer was constructed using electrospinning, resulting in an irregular fiber direction that may contribute to the adhesion and growth of fibroblasts and nerve cells, potentially boosting the regeneration and remodeling of blood vessels in vivo.

Peripheral nerve and vascular regeneration are complicated process that involves the formation of new blood vessels and nerve fibers.[32,33] Our study showed the emergence of nourishing vessels and nerve fibers surrounding the blood vessels during the reconstruction process, which formed a functional complex extending into the smooth muscle of the middle layer (Figure 5A). A significant enhancement was observed in vascular contractile function after reconstruction, signifying the physiological function of the nerve fiber and the integration of the vascular graft into the "living" tissue of the body.

Supported by the robust three-layer structure, the long-term patency rate of the biomimetic blood vessel after reconstruction was analyzed by color Doppler ultrasound and CT

https://doi.org/10.1021/acsomega.3c06628
ACS Omega 2024, 9, 7609−7620

Scheme 1. Sequence and Assumption of Biological Reconstruction[a]

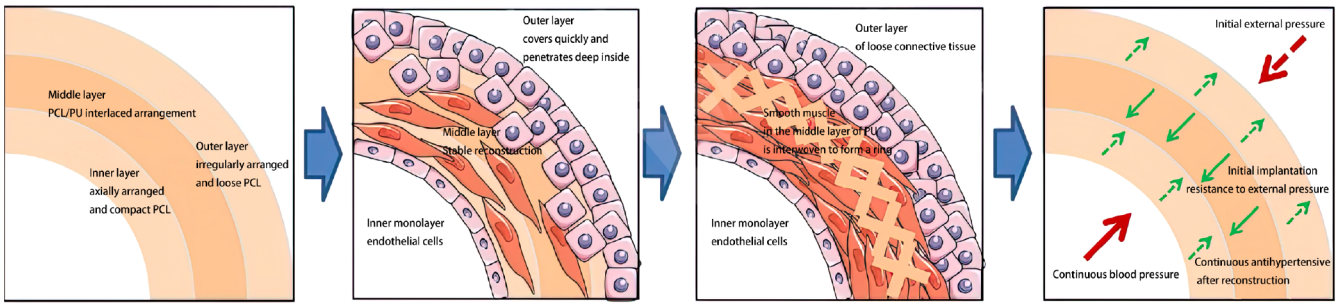

[a]M1 macrophages initially infiltrate the inner and outer layers. M2 polarization and PCL fiber degradation facilitate endothelial cell regeneration in the inner layer and connective tissue coverage in the outer layer. The middle layer, supported by PU fibers, withstands blood pressure and maintains mechanical properties. This promotes smooth muscle growth, resulting in a "live" blood vessel with single-layer endothelial cells interiorly and loose connective tissue exteriorly. Smooth muscle interwoven with PU fibers mimics natural tissue structure and supports physiological regulation.

contrast reconstruction (Figure 5B). At 180 days postsurgery, the rats (n = 3) growth rate showed good patency (Figure 5D) with no signs of lesions, stenosis, or obstruction. Additionally, the blood flow rate remained stable at around 40 cm/s, achieving practical needs of clinical applications.

4. DISCUSSION

The native aorta possesses a three-layer structure that is crucial for its normal function.[1,34] The inner layer consists of tightly packed monolayer endothelial cells, reducing the likelihood of thrombosis and promoting smooth blood flow.[35] On the other hand, the middle layer is composed of annularly arranged smooth muscle cells and elastic membranes, the former achieves vasoconstriction and the latter tolerates blood pressure to prevent excessive expansion of the diameter, which is an important factor for long-term patency of blood vessels.[36] Finally, the outer layer contains blood vessels and nerves, which nourish and regulate blood vessel functions (Scheme 1).

Previous studies attempted to enhance biocompatibility, as well as minimize the risk of embolism and anticoagulant properties to maintain blood vessel patency, which is key for vascular function.[37,38] However, passive reduction of platelet adhesion and activation via modified heparin or other anticoagulant drugs has limited long-term efficacy.[39] Recent research has emphasized the critical role of vascular endothelial cells in maintaining blood flow through physical barriers, metabolic functions, and secretion of regulatory factors such as NO. While loading vascular endothelial growth factors or using an acellular matrix can swiftly form endothelium, safety concerns and limitations still exist in transforming growth into a physiological structure. According to current studies, constructing nanostructures along the inner surface of vascular grafts can impact anticoagulation by controlling the directional growth of cells and hemodynamics.[40,41] In our developed three-layer biomimetic vascular graft, the inner layer featured a sequential microstructure along the blood flow direction, promoting the directional growth of endothelial cells and transformation into the vascular endothelium according to the physiological structure in vivo, ensuring blood flow patency.

Furthermore, prior research has examined the influence of mechanical factors, such as blood pressure, on the constituents of the native aorta and related illnesses.[42] Aberrant blood pressure can impair the functions of endothelial cells in the intima, resulting in thrombosis.[43] Additionally, abnormal blood pressure can also cause smooth muscle cell proliferation, hypertrophy, and remodeling in the middle layer, as well as atypical proliferation and activity of fibrous cells, leading to excessive deposition of type I collagen, lower vascular compliance, and increased peripheral resistance.[44] Notably, uncontrolled blood pressure can lead to fibroblast migration, thereby causing irreversible damage to the vascular wall structure and function. It can also result in changes in the proportion and function of pericytes, leading to vascular regulation disorders. However, there is a paucity of studies investigating the impact of hemodynamics on aortic grafts.[45] Herein, a three-layer biomimetic vascular graft with a ring-shaped structure in the middle layer was developed to promote smooth muscle cell growth while mechanical properties were adjusted during reconstruction. This approach ensured vascular compliance similar to the native aorta, reducing the incidence of mechanical-stress-related adverse effects such as blood pressure on reconstruction and preventing complications to ensure blood flow patency.

Recent research has demonstrated that nerves surrounding blood vessels have a crucial impact on vascular development and repair.[46,47] Nerves and blood vessels simultaneously expand during vascular development, and secreted factors enable mutual regulation between nerve and vascular progenitor cells.[48−50] Effective integration of nerve fibers and smooth muscle cells is a prerequisite for proper vascular regeneration during repair. In cases of adverse stress or infection, fibrosis, and scar formation may occur, which lack neuro-regulation and contractile function, potentially leading to embolism, aneurysms, and other lesions.[51] In the proposed three-layer biomimetic vascular graft, the outer layer of the graft mimics nerve fibers and penetrates the smooth muscle layer to mediate vascular function, enabling functional vascular repair.

We speculate that the impact of the proposed three-layer biomimetic vascular graft on tissue growth and remodeling sequence is closely related to its long-term patency rate.[52,53] The inner and outer layers are composed of degradable PCL, while the middle layer is composed of degradable PCL and nondegradable PU. As PCL degrades, the pores gradually increase, providing space for the infiltration of endothelial cells of the inner layer, forming a smooth and biologically active lining during this process.[54,55] The degradation of the PCL of the outer layer leads to the formation of more pores, providing channels for pericytes and nerves. This structure facilitates the

https://doi.org/10.1021/acsomega.3c06628
ACS Omega 2024, 9, 7609−7620

gradual integration of surrounding cells and tissues, allowing the artificial blood vessel to seamlessly connect with the surrounding environment, while the middle layer is composed of degradable PCL and nondegradable PU. As PCL degrades, the pores gradually increase, providing a growth channel for the smooth muscle cells in the middle layer, forming a resilient middle layer.[56]

Thus, by considering the dynamic requirements of biocompatibility and biomechanics during the tissue remodeling process in the body and influencing the order of tissue remodeling, generating "living" blood vessels that mimic the tissue structure and physiological regulation function of the native aorta is achievable.

5. CONCLUSIONS

In this study, a three-layer arterial graft was developed, providing the blood vessel with sufficient mechanical support and stability through nondegradable PU, as well as potential gaps for tissue ingrowth with degradable PCL, making our graft a living transplant.

■ ASSOCIATED CONTENT

Supporting Information

The Supporting Information is available free of charge at https://pubs.acs.org/doi/10.1021/acsomega.3c06628.

Mechanical properties of biomimetic blood vessels (Figure S1) (PDF)

■ AUTHOR INFORMATION

Corresponding Authors

Fuwei Liu − *State Key Laboratory of Oral & Maxillofacial Reconstruction and Regeneration, National Clinical Research Center for Oral Diseases, Shaanxi Clinical Research Center for Oral Diseases, Department of Oral and Maxillofacial Surgery, School of Stomatology, The Fourth Military Medical University, Xi'an 710032, China;* orcid.org/0000-0001-8942-6697; Email: lfw0912@163.com

Yong Zhao − *Key Laboratory of Bio-inspired Smart Interfacial Science and Technology of Ministry of Education, School of Chemistry, Beihang University, Beijing 100191, China;* orcid.org/0000-0002-2545-1620; Email: zhaoyong@buaa.edu.cn

Liang Kong − *State Key Laboratory of Oral & Maxillofacial Reconstruction and Regeneration, National Clinical Research Center for Oral Diseases, Shaanxi Clinical Research Center for Oral Diseases, Department of Oral and Maxillofacial Surgery, School of Stomatology, The Fourth Military Medical University, Xi'an 710032, China*; Email: liangkong2014@163.com

Authors

Han Bao − *State Key Laboratory of Oral & Maxillofacial Reconstruction and Regeneration, National Clinical Research Center for Oral Diseases, Shaanxi Clinical Research Center for Oral Diseases, Department of Oral and Maxillofacial Surgery, School of Stomatology, The Fourth Military Medical University, Xi'an 710032, China;* orcid.org/0009-0008-9493-0511

Yanyuan Zhang − *State Key Laboratory of Oral & Maxillofacial Reconstruction and Regeneration, National Clinical Research Center for Oral Diseases, Shaanxi Clinical Research Center for Oral Diseases, Department of Oral and Maxillofacial Surgery, School of Stomatology, The Fourth Military Medical University, Xi'an 710032, China*

He Xin − *State Key Laboratory of Oral & Maxillofacial Reconstruction and Regeneration, National Clinical Research Center for Oral Diseases, Shaanxi Clinical Research Center for Oral Diseases, Department of Oral and Maxillofacial Surgery, School of Stomatology, The Fourth Military Medical University, Xi'an 710032, China*

Ye Gao − *State Key Laboratory of Oral & Maxillofacial Reconstruction and Regeneration, National Clinical Research Center for Oral Diseases, Shaanxi Clinical Research Center for Oral Diseases, Department of Oral and Maxillofacial Surgery, School of Stomatology, The Fourth Military Medical University, Xi'an 710032, China*

Yan Hou − *State Key Laboratory of Oral & Maxillofacial Reconstruction and Regeneration, National Clinical Research Center for Oral Diseases, Shaanxi Clinical Research Center for Oral Diseases, Department of Oral and Maxillofacial Surgery, School of Stomatology, The Fourth Military Medical University, Xi'an 710032, China*

Guichu Yue − *Key Laboratory of Bio-inspired Smart Interfacial Science and Technology of Ministry of Education, School of Chemistry, Beihang University, Beijing 100191, China;* orcid.org/0000-0002-4398-7410

Nü Wang − *Key Laboratory of Bio-inspired Smart Interfacial Science and Technology of Ministry of Education, School of Chemistry, Beihang University, Beijing 100191, China*

Yaqiong Wang − *Key Laboratory of Bio-inspired Smart Interfacial Science and Technology of Ministry of Education, School of Chemistry, Beihang University, Beijing 100191, China*

Chun Li − *Shandong Nafeibo Technology Development Co., Ltd, Yantai 264000, China*

Complete contact information is available at: https://pubs.acs.org/10.1021/acsomega.3c06628

Author Contributions

‖H.B., Y.Z., and H.X. contributed equally to this work.

Notes

The authors declare no competing financial interest.

■ ACKNOWLEDGMENTS

This work was supported by the top-notch project of the military Medical Science and Technology Youth training Program of the Fourth Military Medical University, China (no. 18QNP029).

■ REFERENCES

(1) Zhang, B.; Montgomery, M.; Chamberlain, M. D.; Ogawa, S.; Korolj, A.; Pahnke, A.; Wells, L. A.; Massé, S.; Kim, J.; Reis, L.; Momen, A.; Nunes, S. S.; Wheeler, A. R.; Nanthakumar, K.; Keller, G.; Sefton, M. V.; Radisic, M. Biodegradable scaffold with built-in vasculature for organ-on-a-chip engineering and direct surgical anastomosis. *Nat. Mater.* **2016**, *15* (6), 669−678.

(2) Dee, P.; You, H. Y.; Teoh, S. H.; Le Ferrand, H. Bioinspired approaches to toughen calcium phosphate-based ceramics for bone repair. *J. Mech. Behav. Biomed. Mater.* **2020**, *112*, 104078.

(3) Ben-Gal, Y.; Gordon, A.; Teich, N.; Sela, O.; Kramer, A.; Ziv-Baran, T.; Mohr, R.; Pevni, D. Saphenous Vein vs Arterial Graft to the Right System in Left-Sided Arterial Revascularization. *Ann. Thorac. Surg.* **2022**, *114* (6), 2280−2287.

(4) Kreeger, P. K.; Strong, L. E.; Masters, K. S. Engineering Approaches to Study Cellular Decision Making. *Annu. Rev. Biomed. Eng.* **2018**, *20*, 49−72.
(5) Wu, W.; Allen, R. A.; Wang, Y. Fast-degrading elastomer enables rapid remodeling of a cell-free synthetic graft into a neoartery. *Nat. Med.* **2012**, *18* (7), 1148−1453.
(6) Vaz, C. M.; van Tuijl, S.; Baaijens, F. P. T. Design of scaffolds for blood vessel tissue engineering using a multi-layering electrospinning technique. *Acta Biomater.* **2005**, *1* (5), 575−582.
(7) McClure, M. J.; Sell, S. A.; Simpson, D. G.; Walpoth, B. H.; Bowlin, G. L. A three-layered electrospun matrix to mimic native arterial architecture using polycaprolactone, elastin, and collagen: A preliminary study. *Acta Biomater.* **2010**, *6* (7), 2422−2433.
(8) Gao, L.; Kupfer, M. E.; Jung, J. P.; Yang, L.; Zhang, P.; Da Sie, Y.; Tran, Q.; Ajeti, V.; Freeman, B. T.; Fast, V. G.; Campagnola, P. J.; Ogle, B. M.; Zhang, J. Myocardial Tissue Engineering With Cells Derived From Human-Induced Pluripotent Stem Cells and a Native-Like, High-Resolution, 3-Dimensionally Printed Scaffold. *Circ. Res.* **2017**, *120* (8), 1318−1325.
(9) Li, S.; Nih, L. R.; Bachman, H.; Fei, P.; Li, Y.; Nam, E.; Dimatteo, R.; Carmichael, S. T.; Barker, T. H.; Segura, T. Hydrogels with precisely controlled integrin activation dictate vascular patterning and permeability. *Nat. Mater.* **2017**, *16* (9), 953−961.
(10) Wynn, T. A.; Vannella, K. M. Macrophages in Tissue Repair, Regeneration, and Fibrosis. *Immunity* **2016**, *44* (3), 450−462.
(11) Hutchings, G.; Janowicz, K.; Moncrieff, L.; Dompe, C.; Strauss, E.; Kocherova, I.; Nawrocki, M. J.; Kruszyna, L.; Wasiatycz, G.; Antosik, P.; Shibli, J. A.; Mozdziak, P.; Perek, B.; Krasinski, Z.; Kempisty, B.; Nowicki, M. The Proliferation and Differentiation of Adipose-Derived Stem Cells in Neovascularization and Angiogenesis. *Int. J. Mol. Sci.* **2020**, *21* (11), 3790.
(12) Yuan, H.; Chen, C.; Liu, Y.; Lu, T.; Wu, Z. Strategies in cell-free tissue-engineered vascular grafts. *J. Biomed. Mater. Res. A* **2020**, *108* (3), 426−445.
(13) Vegas, A. J.; Veiseh, O.; Doloff, J. C.; Ma, M.; Tam, H. H.; Bratlie, K.; Li, J.; Bader, A. R.; Langan, E.; Olejnik, K.; Fenton, P.; Kang, J. W.; Hollister-Locke, J.; Bochenek, M. A.; Chiu, A.; Siebert, S.; Tang, K.; Jhunjhunwala, S.; Aresta-Dasilva, S.; Dholakia, N.; Thakrar, R.; Vietti, T.; Chen, M.; Cohen, J.; Siniakowicz, K.; Qi, M.; McGarrigle, J.; Graham, A. C.; Lyle, S.; Harlan, D. M.; Greiner, D. L.; Oberholzer, J.; Weir, G. C.; Langer, R.; Anderson, D. G. Combinatorial hydrogel library enables identification of materials that mitigate the foreign body response in primates. *Nat. Biotechnol.* **2016**, *34* (3), 345−352.
(14) Hibino, N.; McGillicuddy, E.; Matsumura, G.; Ichihara, Y.; Naito, Y.; Breuer, C.; Shinoka, T. Late-term results of tissue-engineered vascular grafts in humans. *J. Thorac. Cardiovasc. Surg.* **2010**, *139* (2), 431−436.
(15) Lagendijk, A. K.; Gomez, G. A.; Baek, S.; Hesselson, D.; Hughes, W. E.; Paterson, S.; Conway, D. E.; Belting, H. G.; Affolter, M.; Smith, K. A.; Schwartz, M. A.; Yap, A. S.; Hogan, B. M. Live imaging molecular changes in junctional tension upon VE-cadherin in zebrafish. *Nat. Commun.* **2017**, *8* (1), 1402.
(16) Jiang, Y.-C.; Wang, X.-F.; Xu, Y.-Y.; Qiao, Y.-H.; Guo, X.; Wang, D.-F.; Li, Q.; Turng, L.-S. Polycaprolactone Nanofibers Containing Vascular Endothelial Growth Factor-Encapsulated Gelatin Particles Enhance Mesenchymal Stem Cell Differentiation and Angiogenesis of Endothelial Cells. *Biomacromolecules* **2018**, *19* (9), 3747−3753.
(17) Vijayavenkataraman, S.; Kannan, S.; Cao, T.; Fuh, J. Y. H.; Sriram, G.; Lu, W. F. 3D-Printed PCL/PPy Conductive Scaffolds as Three-Dimensional Porous Nerve Guide Conduits (NGCs) for Peripheral Nerve Injury Repair. *Front. Bioeng. Biotechnol.* **2019**, *7*, 266.
(18) Li, Z.; Tan, B. H. Towards the development of polycaprolactone based amphiphilic block copolymers: Molecular design, self-assembly and biomedical applications. *Mater. Sci. Eng. C Mater. Biol. Appl.* **2014**, *45*, 620−634.
(19) Zhou, J.; Ying, H.; Wang, M.; Su, D.; Lu, G.; Chen, J. Dual layer collagen-GAG conduit that mimic vascular scaffold and promote blood vessel cells adhesion, proliferation and elongation. *Mater. Sci. Eng. C Mater. Biol. Appl.* **2018**, *92*, 447−452.
(20) Luraghi, A.; Peri, F.; Moroni, L. Electrospinning for drug delivery applications: A review. *J. Controlled Release* **2021**, *334*, 463−484.
(21) L'Heureux, N.; Dusserre, N.; Konig, G.; Victor, B.; Keire, P.; Wight, T. N.; Chronos, N. A.; Kyles, A. E.; Gregory, C. R.; Hoyt, G.; Robbins, R. C.; McAllister, T. N. Human tissue-engineered blood vessels for adult arterial revascularization. *Nat. Med.* **2006**, *12* (3), 361−365.
(22) Yamamoto, K.; Sokabe, T.; Matsumoto, T.; Yoshimura, K.; Shibata, M.; Ohura, N.; Fukuda, T.; Sato, T.; Sekine, K.; Kato, S.; Isshiki, M.; Fujita, T.; Kobayashi, M.; Kawamura, K.; Masuda, H.; Kamiya, A.; Ando, J. Impaired flow-dependent control of vascular tone and remodeling in P2 × 4-deficient mice. *Nat. Med.* **2006**, *12* (1), 133−137.
(23) Zong, X.; Bien, H.; Chung, C. Y.; Yin, L.; Fang, D.; Hsiao, B. S.; Chu, B.; Entcheva, E. Electrospun fine-textured scaffolds for heart tissue constructs. *Biomaterials* **2005**, *26* (26), 5330−5338.
(24) Wu, S.; Dong, T.; Li, Y.; Sun, M.; Qi, Y.; Liu, J.; Kuss, M. A.; Chen, S.; Duan, B. State-of-the-art review of advanced electrospun nanofiber yarn-based textiles for biomedical applications. *Appl. Mater. Today* **2022**, *27*, 101473.
(25) Frangogiannis, N. G. Cardiac fibrosis. *Cardiovasc. Res.* **2021**, *117* (6), 1450−1488.
(26) Bonnans, C.; Chou, J.; Werb, Z. Remodelling the extracellular matrix in development and disease. *Nat. Rev. Mol. Cell Biol.* **2014**, *15* (12), 786−801.
(27) Campbell, I. D.; Humphries, M. J. Integrin structure, activation, and interactions. *Cold Spring Harb Perspect. Biol.* **2011**, *3* (3), a004994.
(28) Shin, M.; Ishii, O.; Sueda, T.; Vacanti, J. P. Contractile cardiac grafts using a novel nanofibrous mesh. *Biomaterials* **2004**, *25* (17), 3717−3723.
(29) Straub, A. C.; Lohman, A. W.; Billaud, M.; Johnstone, S. R.; Dwyer, S. T.; Lee, M. Y.; Bortz, P. S.; Best, A. K.; Columbus, L.; Gaston, B.; Isakson, B. E. Endothelial cell expression of haemoglobin alpha regulates nitric oxide signalling. *Nature* **2012**, *491* (7424), 473−477.
(30) Qiu, Y.; Zhang, C.; Zhang, G.; Tao, J. Endothelial progenitor cells in cardiovascular diseases. *Aging Med.* **2018**, *1* (2), 204−208.
(31) Burnstock, G. Autonomic neurotransmission: 60 years since sir Henry Dale. *Annu. Rev. Pharmacol. Toxicol.* **2009**, *49*, 1−30.
(32) Veith, A. P.; Henderson, K.; Spencer, A.; Sligar, A. D.; Baker, A. B. Therapeutic strategies for enhancing angiogenesis in wound healing. *Adv. Drug Delivery Rev.* **2019**, *146*, 97−125.
(33) Johnson, E. O.; Charchanti, A.; Soucacos, P. N. Nerve repair: Experimental and clinical evaluation of neurotrophic factors in peripheral nerve regeneration. *Injury* **2008**, *39*, 37−42.
(34) Shin'oka, T.; Matsumura, G.; Hibino, N.; Naito, Y.; Watanabe, M.; Konuma, T.; Sakamoto, T.; Nagatsu, M.; Kurosawa, H. Midterm clinical result of tissue-engineered vascular autografts seeded with autologous bone marrow cells. *J. Thorac. Cardiovasc. Surg.* **2005**, *129* (6), 1330−1338.
(35) Carrabba, M.; Madeddu, P. Current Strategies for the Manufacture of Small Size Tissue Engineering Vascular Grafts. *Front. Bioeng. Biotechnol.* **2018**, *6*, 41.
(36) Fayon, A.; Menu, P.; El Omar, R. Cellularized small-caliber tissue-engineered vascular grafts: Looking for the ultimate gold standard. *NPJ. Regener Med.* **2021**, *6* (1), 46.
(37) Burmester, G. R.; Pope, J. E. Novel treatment strategies in rheumatoid arthritis. *Lancet* **2017**, *389* (10086), 2338−2348.
(38) Chen, G. Y.; Nunez, G. Sterile inflammation: Sensing and reacting to damage. *Nat. Rev. Immunol* **2010**, *10* (12), 826−837.
(39) Gabrilovich, D. I.; Nagaraj, S. Myeloid-derived suppressor cells as regulators of the immune system. *Nat. Rev. Immunol* **2009**, *9* (3), 162−174.
(40) Lee, D. M.; Weinblatt, M. E. Rheumatoid arthritis. *Lancet* **2001**, *358* (9285), 9903−11.

https://doi.org/10.1021/acsomega.3c06628
ACS Omega 2024, 9, 7609−7620

(41) Firestein, G. S.; McInnes, I. B. Immunopathogenesis of Rheumatoid Arthritis. *Immunity* **2017**, *46* (2), 183−196.
(42) Fraenkel, L.; Bathon, J. M.; England, B. R.; St Clair, E. W.; Arayssi, T.; Carandang, K.; Deane, K. D.; Genovese, M.; Huston, K. K.; Kerr, G.; Kremer, J.; Nakamura, M. C.; Russell, L. A.; Singh, J. A.; Smith, B. J.; Sparks, J. A.; Venkatachalam, S.; Weinblatt, M. E.; Al-Gibbawi, M.; Baker, J. F.; Barbour, K. E.; Barton, J. L.; Cappelli, L.; Chamseddine, F.; George, M.; Johnson, S. R.; Kahale, L.; Karam, B. S.; Khamis, A. M.; Navarro-Millan, I.; Mirza, R.; Schwab, P.; Singh, N.; Turgunbaev, M.; Turner, A. S.; Yaacoub, S.; Akl, E. A. 2021 American College of Rheumatology Guideline for the Treatment of Rheumatoid Arthritis. *Arthritis Rheumatol.* **2021**, *73* (7), 1108−1123.
(43) Schermuly, R. T.; Ghofrani, H. A.; Wilkins, M. R.; Grimminger, F. Mechanisms of disease: Pulmonary arterial hypertension. *Nat. Rev. Cardiol,* **2011**, *8* (8), 443−455.
(44) Ramirez-Perez, F. I.; Woodford, M. L.; Morales-Quinones, M.; Grunewald, Z. I.; Cabral-Amador, F. J.; Yoshida, T.; Brenner, D. A.; Manrique-Acevedo, C.; Martinez-Lemus, L. A.; Chandrasekar, B.; Padilla, J. Mutation of the 5′-untranslated region stem-loop mRNA structure reduces type I collagen deposition and arterial stiffness in male obese mice. *Am. J. Physiol. Heart Circ. Physiol.* **2021**, *321* (2), H435−H445.
(45) He, L.; Zhang, C.-L.; Chen, Q.; Wang, L.; Huang, Y. Endothelial shear stress signal transduction and atherogenesis: From mechanisms to therapeutics. *Pharmacol. Ther.* **2022**, *235*, 108152.
(46) de Oliveira, S.; Rosowski, E. E.; Huttenlocher, A. Neutrophil migration in infection and wound repair: Going forward in reverse. *Nat. Rev. Immunol.* **2016**, *16* (6), 378−391.
(47) Kawai, T.; Akira, S. Toll-like receptors and their crosstalk with other innate receptors in infection and immunity. *Immunity* **2011**, *34* (5), 637−650.
(48) Day, R. B.; Link, D. C. Regulation of neutrophil trafficking from the bone marrow. *Cell. Mol. Life Sci.* **2012**, *69* (9), 1415−1423.
(49) Taneja, R.; Parodo, J.; Jia, S. H.; Kapus, A.; Rotstein, O. D.; Marshall, J. C. Delayed neutrophil apoptosis in sepsis is associated with maintenance of mitochondrial transmembrane potential and reduced caspase-9 activity. *Crit. Care Med.* **2004**, *32* (7), 1460−1469.
(50) Abraham, E. Neutrophils and acute lung injury. *Crit. Care Med.* **2003**, *31* (4 Suppl), S195−S199.
(51) Rehman, J.; Li, J.; Orschell, C. M.; March, K. L. Peripheral blood ″endothelial progenitor cells″ are derived from monocyte/macrophages and secrete angiogenic growth factors. *Circulation* **2003**, *107* (8), 1164−1169.
(52) Stewart, C.; Akhavan, B.; Wise, S. G.; Bilek, M. M. M. A review of biomimetic surface functionalization for bone-integrating orthopedic implants: Mechanisms, current approaches, and future directions. *Prog. Mater. Sci.* **2019**, *106*, 100588.
(53) Brown, R. A.; Phillips, J. B. Cell responses to biomimetic protein scaffolds used in tissue repair and engineering. *Int. Rev. Cytol.* **2007**, *262*, 75−150.
(54) Gaharwar, A. K.; Singh, I.; Khademhosseini, A. Engineered biomaterials for in situ tissue regeneration. *Nat. Rev. Mater.* **2020**, *5* (9), 686−705.
(55) Wu, Y. Electrohydrodynamic jet 3D printing in biomedical applications. *Acta Biomater.* **2021**, *128*, 21−41.
(56) Liu, K.; Wang, N.; Wang, W.; Shi, L.; Li, H.; Guo, F.; Zhang, L.; Kong, L.; Wang, S.; Zhao, Y. A bio-inspired high strength three-layer nanofiber vascular graft with structure guided cell growth. *J. Mater. Chem. B* **2017**, *5* (20), 3758−3764.

https://doi.org/10.1021/acsomega.3c06628
ACS Omega 2024, 9, 7609−7620